# Toughening poly(lactide) with bio-based poly(farnesene) elastomers

Matthew W. Halloran,[1] Jim A. Nicell,[2] Richard L. Leask,[1] Milan Marić*[1]

[1]Department of Chemical Engineering, McGill University, 3610 University Street, Montréal, QC, Canada, H3A 0C5

[2]Department of Civil Engineering, McGill University, 817 Sherbrooke Street West, Montreal, Quebec, Canada, H3A 0C3

*corresponding author:
milan.maric@mcgill.ca
tel +1(514) 398-4272
fax +1(514) 398-6678

## Abstract

The development and application of bio-sourced elastomers which can be blended with poly(lactide) (PLA) to enhance its poor material properties are of great interest as we move towards replacing petroleum-derived plastics with viable alternatives. As such, this work focused on the valorization of the terpene-based monomer, trans-β-farnesene (*Far*), as a building block to design rubber toughening agents to improve the impact strength of PLA blends. Ternary blends consisting of copolymers of *Far*-glycidyl methacrylate (PFGMA), *Far*-methacrylic acid (PFMAA) (20-30 wt% Far-copolymers), and PLA exhibited significant improvements in impact strength and elongation at break (i.e., approximately 16-fold and 10-fold, respectively) over neat PLA. Torque mixer measurements and FTIR spectroscopy confirmed the occurrence of epoxy-acid/epoxy-hydroxyl interfacial compatibilization reactions catalyzed through hydrogen bonding interactions. Phase morphologies of the ternary blends were evaluated with scanning electron microscopy (SEM) and showed an approximate 4-fold reduction in particle diameter relative to the binary systems (i.e., from 4.3 to 1.1 μm) with the compatibilized blend morphology deemed stable upon annealing. The toughening mechanism responsible for the improved mechanical properties observed with the ternary blends was also investigated by examining the impact fractured surface morphologies with SEM. A combination of enhanced interfacial adhesion coupled with shear yielding of the matrix was proposed as the main contributing factor to the improvement in mechanical properties observed in the ternary blends.

**Key words:** poly(lactide), bio-based elastomer, toughening, ternary blend, reactive blending

# Introduction

As a renewably sourced and biodegradable polymer, poly(lactide) (PLA) has been shown to be a promising alternative to petroleum-derived poly(styrene) (PS) and poly(ethylene terephthalate) (PET).[1] Owing to its high tensile strength and modulus, PLA has been found suitable for applications in the packaging industry[2] and the biomedical field where it is used to manufacture implantable medical devices and degradable sutures.[3, 4] Nevertheless, PLA suffers from several shortcomings such as its inherent brittleness and poor tensile properties which have restricted its widespread use as a viable replacement for PET or PS.[5] To address these shortcomings, the most commonly adopted methods to improve the mechanical properties of PLA are through the incorporation of plasticizers which help to lower the glass transition temperature ($T_g$) of the blend while imparting flexibility,[6] and through blending with an immiscible rubbery polymer to enhance impact toughness.[7]

The latter approach has received considerable attention over the last two decades due to its low cost, efficiency, and ability to fine-tune the mechanical properties by altering the components and composition of the blend.[8, 9] However, achieving adequate compatibilization between PLA and the rubbery phase is not straightforward,[10] and often requires the use of suitable graft or copolymers which can be pre-made or formed *in situ* through reactive compatibilization.[11] In this context, many reports have demonstrated significant improvements in the impact strength and tensile properties of PLA by incorporating poly(ethylene) (PE),[12] acrylonitrile-butadiene-styrene copolymer,[13] poly(ε-caprolactone),[14] poly(butylene succinate),[15] poly(carbonate),[16] and ethylene-glycidyl-methacrylate (EGMA),[17] just to name a few. Despite the excellent mechanical properties obtained with these systems, the use of these additives compromises the sustainable nature of PLA due to their petroleum-derived origins. Consequently, focus has shifted towards toughening PLA with renewably sourced polymers[18] such as natural rubbers,[19, 20] polyhydroxybutyrates,[21] epoxidized corn[22] or soybean oils,[23] and lignocellulosic biomass.[24-26]

Alternatively, terpene-based monomers such as β-myrcene (*Myr*) and trans-β-farnesene (*Far*) have emerged as promising building blocks for the development of renewably sourced rubbery materials[27] which exhibit similar properties to poly(isoprene) and poly(butadiene).[28, 29] Both poly(*Myr*) and poly(*Far*) display similarly low $T_g$s (i.e., ~ -70 °C) in comparison to poly(butadiene) (i.e., with a $T_g$ of -100 °C), while their bottlebrush-like structure with densely-packed, long side chains establishes them as excellent candidates as bio-based elastomeric materials.[30-33] As a

naturally-occurring compound found in many essential oils, *Far* can also be produced on large scale from sugar cane fermentation.[34]

Although previous work has demonstrated the effectiveness of *Myr* graft copolymers to improve the mechanical properties of both poly(urethane)[35] and PLA,[36] to the best of our knowledge the use of poly(*Far*) as an additive in such applications has not been previously explored. Therefore, this work describes the synthesis and evaluation of functionalized poly(*Far*) derivatives as renewably-sourced elastomeric rubber toughening agents in blends with PLA. The rheological, morphological, thermal, and mechanical properties of the blends was investigated as both binary and ternary mixtures with the overarching goal of achieving compatibilization in conjunction with targeting an increase in impact strength. *Far* copolymers containing modest amounts (10 mol%) of glycidyl methacrylate (GMA) and methacrylic acid (MAA) functionalities were also evaluated as potential reactive compatibilizers for poly(*Far*)/PLA blends which could undergo cross-linking reactions through an acid-epoxy, or transesterification reaction. It was subsequently demonstrated through torque mixer measurements and FTIR spectroscopy that epoxy-acid/epoxy-hydroxyl cross-linking reactions catalyzed through intermolecular hydrogen-bonding interactions occurred in the ternary blends during melt-mixing. This work demonstrates the potential of poly(*Far*) to serve as an effective bio-based elastomeric toughening agent for PLA.

# Materials and Methods

## Materials and Reagents

Poly(lactide) (Ingeo Bioworks 2003D, MFI = 6 g/10min (210 °C/2.16 kg) and density = 1.24 g/cm$^3$) was purchased from Nature-Works LLC (Minnetonka, MN). Trans-β-farnesene, or Biofene (*Far,* ≥95%), was generously donated by Amyris with thanks to Derek McPhee (Emeryville, CA). Glycidyl methacrylate (GMA, 97%), methacrylic acid (MAA, 99%), deuterated chloroform ($CDCl_3$), and dicumyl peroxide (DCP, 98%) were purchased from Sigma Aldrich (Oakville, ON). The monomers were purified using 1.0 g of aluminum oxide (basic $Al_2O_3$, activated, Brockmann I) and 0.05 g calcium hydride (≥90%) per 50 mL of monomer. Xylenes (ACS grade), chloroform (ACS grade), and tetrahydrofuran (HPLC grade) were purchased from Fisher Scientific (Montreal, QC).

## Experimental Methods

*Synthesis of poly(Far) additives*

Poly(*Far*) (PF) was synthesized via conventional free radical polymerization in accordance with a slightly modified version of a previously reported procedure,[37] wherein the reaction was conducted in 50 weight% xylenes (w.r.t. *Far* monomer) instead of in bulk, and the reaction time was increased to 12 hours. Poly(*Far*-co-glycidyl methacrylate) (PFGMA) and poly(*Far*-co-methacrylic acid) (PFMAA) were synthesized under analogous conditions using 10 mol% of glycidyl methacrylate and methacrylic acid, respectively. Hydrogenated poly(*Far*) (HPF) was synthesized according to a previously reported procedure.[37] Monomer conversions were calculated using $^1$H NMR as previously described.[37] The copolymer composition was equal to the initial monomer composition in the reaction.

*Melt Mixing of blends*

Melt-mixed blends were prepared using a Rheocord System 40 double arm internal batch mixer (Haake Buchler). The PLA pellets and *Far* polymers were dried under vacuum for 24 hours at 50 °C to remove residual moisture before use. Batches of 50 g each blend were pre-weighed and were briefly stirred manually with a spatula before being added to the batch mixer and mixed for 6 minutes at 175 °C with a rotation rate of 100 rpm. The batches were then quenched into a liquid

nitrogen bath to freeze the morphology and stored for further analysis. Neat PLA was processed under the same conditions for comparison purposes.

*Compression Molding of Mechanical Test Bars*

Test bars of blends were produced with compression molding using a heated manual hydraulic press (Carver Manual Hydraulic Press with Watlow temperature controllers, St. Louis, MO) and steel molds. Blends were cut into small fragments and dried in a vacuum oven at 50 °C for 24 hours before being placed into the molds and pressed at 175 °C for 5 minutes at 10 metric tonnes. Tensile test bar dimensions were as follows: a thickness (*T*) of 1.4 mm; a width of narrow section (*W*) of 3.3 mm; a length of narrow section (*L*) of 17.8 mm; an overall length of 64 mm; and an overall width of 10 mm. Bars for impact testing with the dimensions of *T*= 3.0 mm, *W*= 12.7 mm, and *L*= 63.5 mm were prepared in the same manner described above. Dynamic thermal mechanical analysis (DMTA) bars were prepared in the same manner with the following dimensions: *T*= 1.45 mm, *L*= 45 mm, and *W*= 10 mm. The exact dimensions (thickness/width) of each specimen were recorded using an electronic caliper prior to testing.

## Characterization Methods

*Mechanical Testing*

Tensile testing was performed using a Shimadzu (Kyoto, Japan) Easy Test instrument equipped with a 500 N load cell in accordance with ASTM standard D638-14. Test bars were aged for 48 hours before being clamped and subjected to a strain rate of 5 mm/min. The stress−strain curves were used to obtain values for strain (% elongation), stress at break, and modulus.

Notched Izod impact strength was measured in accordance with ASTM standard D256 using a CEAST Universal Pendulum Impact tester. A minimum of 5 specimens were tested per blend for both tensile and Izod testing.

*Scanning Electron Microscopy (SEM)*

The morphology of the samples was investigated with scanning electron microscopy (SEM), using a FEI Quanta 450 Environmental Scanning Electron Microscope (FE-ESM) operating under high vacuum and acceleration voltage of 10.0 kV. Binary blends were freeze-fractured with liquid nitrogen, while ternary blends were cryo-microtomed using Leica Microsystems EM UC7/FC7 cryo-ultramicrotome (Leica Microsystems, Wetzlar, Germany) with a Diatome diamond knife (Diatome, Nidau, Switzerland) at -120 °C. Cryo-microtomy was used to prepare samples of the

ternary blends to obtain higher quality images for particle analysis as images of the freeze-fractured surfaces did not provide enough contrast between phases. All samples were mounted on aluminum stubs with carbon tape and then sputter-coated with 4 nm of platinum prior to analysis using a Leica Microsystems EM ACE600 High Resolution Sputter Coater. Particle analysis was performed using Fiji-ImageJ software to obtain cross-sectional particle areas that were converted to an equivalent sphere diameter. At least 300 particles from four independent SEM images were measured for each blend to ensure reliable statistics. Weight-average particle diameter ($d_w$) was calculated according to equation (1):

$$d_w = \frac{\sum n_i d_i^2}{\sum n_i d_i} \qquad (1)$$

where $n_i$ is the number of particles with diameter $d_i$. The particle size polydispersity was calculated as the ratio of weight-average particle diameter to number average particle diameter ($d_n$), i.e., $d_w/d_n$. Selected impact-fractured specimens were also evaluated with SEM to investigate the toughening mechanism by imaging sections adjacent to the notch. Selected samples were thermally annealed above the $T_g$ of PLA at 100 °C in a vacuum oven for 8 hours and imaged to evaluate blend stability. The blends were deemed stable if the dispersed phase particle size did not increase by more than 20% after thermal annealing.[38]

*Thermal Gravimetric Analysis (TGA)*

The thermal stability of the homopolymers and blends was evaluated using a TA Instruments Discovery 5500 (New Castle, DE) instrument under nitrogen flow of 25 mL/min from 25 to 500 °C at a heating rate of 10 °C/min. The onset temperature at weight loss with 10% ($T_{10}$) is reported for comparison purposes.

*Differential Scanning Calorimetry (DSC)*

The glass transition temperature ($T_g$) of homopolymers and blends were measured by differential scanning calorimetry (DSC) using a TA Instruments Q2000 (New Castle, DE) under a nitrogen atmosphere using a heat/cool/heat cycle. The samples were heated from 25-170 °C at a rate of 20 °C per minute, held constant at 170 °C for two minutes, then cooled to -90 °C at a rate of 10 °C per minute and held constant for two minutes at -90 °C. The samples were then heated to 170 °C at a rate of 20 °C per minute. The $T_g$ was then determined from the reversible heat flow of the second heating cycle using the automated glass/step transition tool in the TA Instruments Universal

Analysis 2000 software. Melting ($T_m$) and cold crystallization ($T_{cc}$) temperatures were taken from the second heating scan. Crystallinity ($X_c$) was calculated using equation (2) below with the melt and crystallization enthalpies where $\Delta H_m$, $\Delta H_{cc}$, $\Delta H_m^0$, and $w_{PLA}$ represent the enthalpy of melting, the enthalpy of cold crystallization, the enthalpy of melting for 100% crystalline PLA, and the weight percent of PLA in the blend, respectively.

$$X_c = \frac{\Delta H_m - \Delta H_{cc}}{\Delta H_m^0 \times w_{PLA}} \times 100\% \quad (2)$$

A value of 93.15 J/g was taken as the melting enthalpy for 100% crystalline PLA.[39]

*Rheology*

Rheological characterization was conducted using an Anton Paar MCR 302 instrument equipped with a CTD 450 convection oven operated under an $N_2$ atmosphere. Frequency sweep measurements of the homopolymers were conducted using a parallel plate (PP 25, diameter of 25 mm) configuration (1 mm gap) at a temperature of 175 °C to replicate blending conditions. Neat PLA pellets were compression molded into disks of 25 mm diameter and 1 mm thickness, while the poly(*Far*) derivatives were directly loaded onto the plate with a spatula. All samples were stabilized for 10 minutes at 175 °C before beginning the test. The homopolymer samples were measured using a shear strain of 1.0% (within the linear viscoelastic range) and frequency range of 0.1 to 100 rad/s to obtain the storage modulus ($G$') and complex viscosity (η*).

*Dynamic Thermal Mechanical Analysis (DMTA)*

Dynamic thermal mechanical analysis (DMTA) was conducted on the blends to evaluate miscibility using the SRF 12 configuration on the MCR 302 instrument with a CTD 450 convection oven operated under an $N_2$ atmosphere. Compression-molded test bars were loaded in tension, and a temperature ramp was performed from 25 to 150 °C at a rate of 5 °C/min, with an oscillation strain of 0.1% and a frequency of 1 Hz to obtain the storage modulus ($G$') and tanδ curves.

*Gel Permeation Chromatography (GPC)*

The poly(*Far*) homopolymers' molecular weight distributions were analyzed using GPC. The number average molecular weight ($M_n$) and dispersity ($Đ = M_w/M_n$) were measured using a Waters

Breeze instrument and HPLC-grade THF as an eluent at a flow rate of 0.3 mL/min. The GPC has three Waters Styragel HR columns (HR1 which has a molecular weight measurement range of $10^2$ to $5 \times 10^3$ g/mol, HR2 with a molecular weight measurement range of $5 \times 10^2$ to $2 \times 10^4$ g/ mol, and HR4 with a molecular weight measurement range of $5 \times 10^3$ to $6 \times 10^5$ g/mol), a guard column, as well as a refractive index (RI 2414) detector. The columns were heated to 40 °C throughout analysis. The molecular weights were determined relative to poly-(methyl methacrylate) (PMMA) calibration standards from Varian Inc. (ranging from 875 to 1,677,000 g/mol). The reported molecular weights were all relative to the PMMA standards and not adjusted with Mark−Houwink parameters for universal calibration.

*Proton Nuclear Magnetic Resonance ($^1$H NMR) Spectroscopy*

$^1$H NMR spectra were collected using a Bruker AVIIIHD 500 MHz spectrometer (MA, USA) with an average of 16 scans using deuterated chloroform ($CDCl_3$) as the solvent.

*Fourier Transform Infrared (FTIR) Spectroscopy*

FTIR measurements were conducted using a Perkin Elmer instrument (Spectrum II series) which is equipped with a single bounce diamond attenuated transmission reflectance (ATR) for solids. 32 scans were recorded for each sample over the range 4000−500 $cm^{-1}$ with a normal resolution of 4 $cm^{-1}$. The *Far* homopolymers were measured as is, whereas neat PLA was solvent cast from chloroform ($CHCl_3$) to produce a thin film for analysis. Ternary blends were stirred in $CHCl_3$ for 48 hours at room temperature to dissolve PLA, PFMAA, and PFGMA, while the cross-linked portions remained insoluble and were collected via syringe and dried. This process was repeated three times to ensure only the cross-linked portions remained before analysis with FTIR. See Supplementary Information, Figure S6, for a picture of the isolated insoluble fractions.

# Results and Discussion

## Synthesis and Characterization of *Far* Polymers

In contrast to poly(isoprene) and poly(butadiene) which have entanglement molecular weights ($M_e$) of 3000-5000 g/mol and 1500-1900 g/mol,[40] respectively, poly(*Far*) has a much higher $M_e$ of 50,000 g/mol due to its repeating unit having a higher degree of unsaturation (i.e. 3 vs. 1).[41]

Therefore, in order to obtain poly(*Far*) samples with similar viscoelastic properties as poly(isoprene) and poly(butadiene) which could be used to rubber toughen PLA, a molecular weight of 50,000 g/mol or higher is required. Conditions for the synthesis of poly(*Far*) have previously been developed using several different approaches including anionic polymerization,[29] redox free-radical polymerization in emulsion,[42] nitroxide-mediated polymerization in miniemulsions[43] and bulk,[44] and free-radical polymerization (FRP).[37] However, only the FRP conditions are generally amenable to synthesize species with molecular weights greater than 50,000 g/mol.

Here, slightly modified FRP conditions from Luk *et al.*[37] were employed to synthesize a suite of high molecular weight ($M_n$'s of 58-63 kg/mol) *Far*-based polymers (Figure 1). The hydrogenated derivative (HPF) has previously been shown to have higher thermal stability, a lower $M_e$, and higher viscosity relative to its unsaturated counterpart (PF),[37, 40] which are all more favorable characteristics of an elastomeric toughening agent for PLA and was therefore of interest here. With the goal of promoting an interfacial compatibilization reaction to achieve enhanced material properties, epoxy (PFGMA) and carboxylic acid (PFMAA) functionalized derivatives were also synthesized under the same conditions containing only modest amounts of compatibilizer (10 mol%). Both epoxy and carboxylic acid groups have been used previously as successful compatibilization agents between immiscible rubbery polymers and PLA to generate toughened blends.[16, 45-49] Glass transition temperatures ($T_g$) of the homopolymers ranged between -58.5 to -71.8 °C, while they all exhibited excellent thermal stabilities as the onset temperatures of 10% mass loss ($T_{d,10\%}$) were all well above 300 °C (Table 1) (See Figures S1 and S2 for DSC and TGA curves).

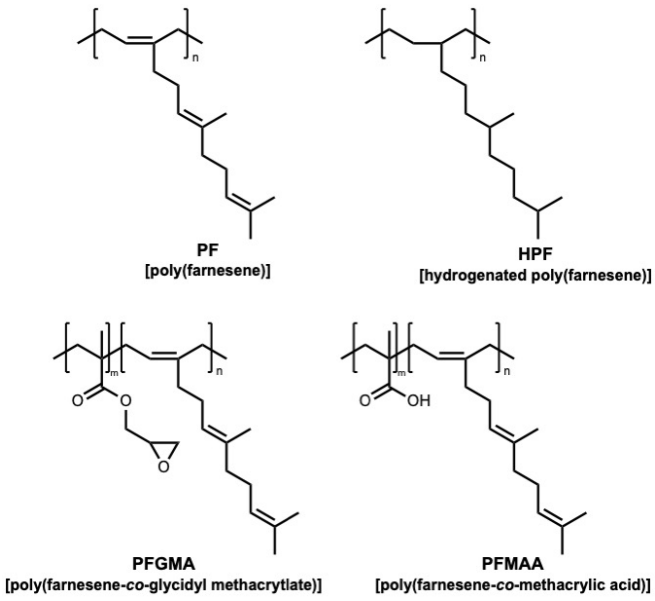


**Figure 1.** Chemical structures of *Far*-based polymers synthesized and used in this study.

**Table 1.** Structural and thermal properties of the synthesized *Far*-based polymers.

| | $M_n$ (kg/mol)[a] | $Đ = M_w/M_n$ | $T_g$ (°C)[b] | $T_{d,10\%}$ (°C)[c] |
|---|---|---|---|---|
| PF | 62 | 6.9 | -71.8 | 331 |
| HPF | 61 | 7.1 | -58.5 | 356 |
| PFGMA (10 mol% GMA) | 63 | 4.2 | -69.8 | 317 |
| PFMAA (10 mol% MAA | 58 | 4.1 | -69.3 | 341 |

[a] Measured with GPC relative to PMMA standards
[b] Measured from the second heating cycle of DSC exotherm
[c] Onset temperature at 10% mass loss measured with TGA

## Rheological Characterization of Homopolymers

The complex viscosity measurements of the homopolymers taken at 175 °C within the linear viscoelastic region were evaluated to predict the rheological properties during melt-blending (Figure 2). At higher frequencies ($\boldsymbol{\omega} > 25$ $s^{-1}$), the four *Far*-containing polymers have similar complex viscosities that range from 11 to 29 Pa·s, which is roughly two orders of magnitude lower

than that of PLA. To minimize particle size of the dispersed phase during polymer blending and achieve optimal blending, the viscosity ratio between the dispersed phase and the host polymer matrix should ideally be near unity.[50] While the viscosity ratio ultimately plays a significant role in obtaining minimal particle size, a significant mismatch in viscosity ratios can be offset through reactive blending between the two immiscible phases to achieve sub-micron particle dispersions.[51, 52] It has been shown that at higher concentrations of the dispersed phase (i.e., >15%), the suppression of droplet coalescence is the dominant contribution of reactive compatibilizers which help to stabilize the interface.[51] Given the discrepancies in viscosities between the *Far* polymers and PLA here, phase separation is expected to occur which will need to be offset through reactive interfacial compatibilization. Moreover, using the Flory-Huggins interaction parameter ($\chi$ = 0.43 at 190 °C) for poly(isoprene)/PLA blends[53] as a reference, we anticipate the formation of large dispersed phase droplets in our system arising from a high degree of immiscibility between PLA and poly(*Far*).

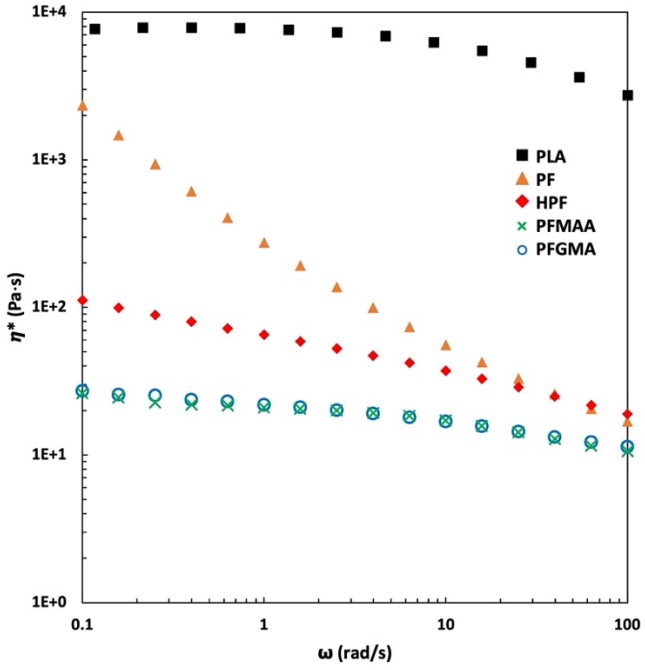


**Figure 2.** Complex viscosity measurements of homopolymers versus frequency measured at 175 °C.

## Mechanical Properties of Blends

The elongation at break and notched impact strength of the blends is shown in Figure 3 and summarized in Table 1. The binary blends exhibited only slight improvements in impact strength (roughly 3-fold) and elongation at break (between 2- and 4-fold) relative to neat PLA at 20 weight % loadings of the *Far* polymers. Compared to neat PLA, a noticeable decrease in the yield stress and elastic modulus was observed in all binary blends, which can be explained by the addition of the soft, rubbery *Far* elastomers. It should also be noted that during testing, the binary blends exhibited distinct yielding before fracture and indicated the enhanced ductility of these blends in relation to neat PLA which underwent brittle fracture. Representative tensile curves are shown in Figure 4 which demonstrate the brittle to ductile transitions observed with the PFGMA, PFMAA binary blends. The negligible improvements in mechanical properties are likely due to the immiscibility between the two phases causing large particle sizes of the dispersed phase inside of the PLA matrix.[54] Large rubber particles have previously been shown to lower the strain at which cavitation can occur, leading to the formation of large holes which promote fracture at low strain rates.[55]

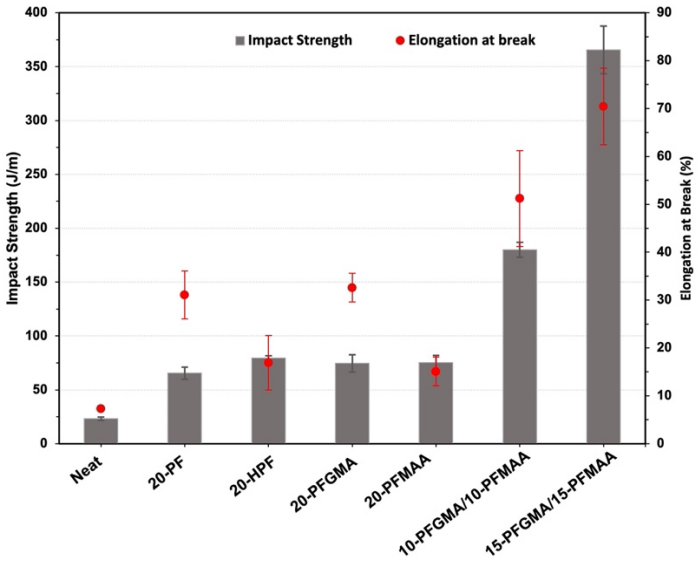


**Figure 3.** Mechanical properties of neat PLA, binary, and ternary blends showing the elongation at break (red dots and dashed line) and notched impact strength (grey bars) ($n$ = 5, error bars represent standard deviation, means are shown).

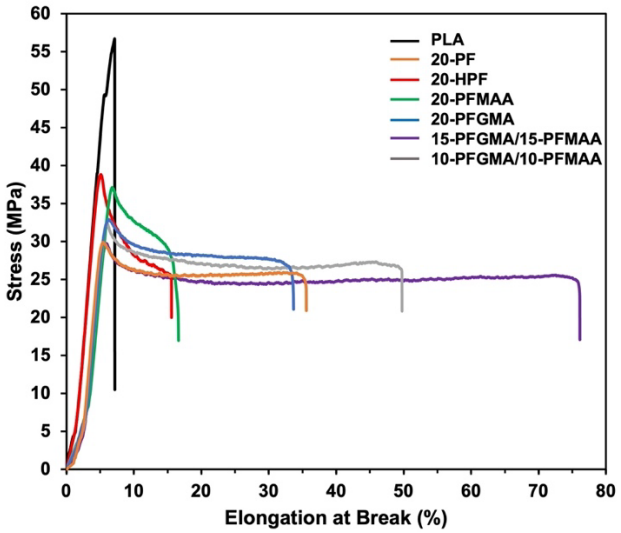


**Figure 4.** Representative strain in elongation at break versus stress curves for the binary and ternary blends.

Evidently, no interfacial compatibilization reactions between the epoxy functionalized PFGMA and the acid/hydroxyl groups on PLA took place under these conditions as all binary blends exhibited similar mechanical properties. Although previous reports have demonstrated the effectiveness of GMA-functionalized polymers as single component impact modifiers of PLA,[17, 49, 56] this proved to not be the case in our system as the incorporation of GMA into the *Far* backbone resulted in only a limited improvement in impact strength relative to neat PLA.

Conversely, the ternary blends consisting of PLA, PFGMA, and PFMAA displayed tremendous improvements in both impact strength and elongation at break. The PLA/(10-PFGMA/10-PFMAA) ternary blend achieved an elongation at break of 51%, and a notched impact strength of 180 J/m, more than 8-fold greater than PLA. Moreover, when the loading was further increased to 30 weight % (15-PFGMA/15-PFMAA in the blend), an impact strength of 366 J/m and elongation at break of 70% was achieved, corresponding to a ~10- and 16-fold increase in elongation at break and impact strength, respectively, over PLA. The improved toughness of the ternary blends was attributed to the occurrence of acid-epoxy/hydroxyl-epoxy cross-linking reactions which took place *in situ* during blending. The cross-linking reactions also led to an improvement in ductility, as both ternary blends demonstrated brittle to ductile transitions accompanied by necking during tensile testing (Figure 4). However, improvement in tensile toughness of rubber toughened blends is often accompanied by a significant decrease in yield strength and elastic modulus relative to the neat polymer.[47] A similar relationship was observed with our ternary blends as the modulus

dropped from ~2200 MPa to ~1500 MPa and the yield stress decreased from ~57 MPa to ~30 MPa with the toughened 15-PFGMA/15PFMA blend. This was also observed in the previous work by Zhou *et al.* using *Myr* grafted PLA blends which demonstrated an elongation at break of 97%, an extremely low elastic modulus of ~70 MPa, and a yield strength of only ~9 MPa.[36]

**Table 2.** Mechanical properties of binary and ternary blends.[a]

| Blend | Yield Stress (MPa) | Elongation at Break (%) | Elastic Modulus (MPa) | Notched Impact Strength (J/m) |
|---|---|---|---|---|
| PLA | 57 ± 0.8 | 7 ± 0.4 | 2210 ± 48 | 22 ± 1 |
| 20-PF | 30 ± 0.6 | 31 ± 5 | 1880 ± 26 | 66 ± 6 |
| 20-HPF | 39 ± 3 | 16 ± 6 | 1930 ± 53 | 80 ± 2 |
| 20-PFGMA | 34 ± 2 | 32 ± 3 | 1870 ± 46 | 75 ± 8 |
| 20-PFMAA | 38 ± 2 | 15 ± 3 | 1880 ± 17 | 75 ± 7 |
| 10-PFGMA/10-PFMAA | 31. ± 0.9 | 51 ± 10 | 1710 ± 24 | 180 ± 8 |
| 15-PFGMA/15-PFMAA | 29 ± 3 | 70 ± 8 | 1530 ± 27 | 366 ± 22 |

[a] Average values reported with standard deviations, n = 5

## Thermal Properties

Previous reports have demonstrated a correlation between the degree of crystallization present in the PLA matrix and the impact strength of the resulting blend.[17, 45] A higher degree of crystallization (>40%), obtained through annealing, was shown to improve impact strength in a system comprised of PLA/poly(ethylene-*co*-glycidyl methacrylate);[17] whereas variations between low levels of crystallinity in other PLA blends (0-6%) was shown to have negligible effects on impact strength.[46, 49, 57, 58] Therefore, to evaluate the role of crystallization on impact strength in our system, the melting ($T_m$) and cold crystallization ($T_{cc}$) temperatures of samples taken from the fractured impact bars were evaluated. Figure 5 shows the DSC exotherms from the first heating cycle of the binary and ternary blends and the values are summarized in Table 3. The exotherms obtained for neat PLA and the prepared blends all exhibit similar thermal transitions, with clear glass transition, crystallization, and melting peaks observed for all species. The difference in melting, cold crystallization, and glass transition temperatures of the blends was not significantly

different than those obtained for neat PLA. Moreover, the toughened 15-PFGMA/15-PFMAA ternary blend had nearly the same crystallinity as neat PLA at 5.9% and did not differ considerably from the other blends. Altogether, these results suggest that crystallinity did not contribute to the enhanced impact strength observed in the ternary blends.

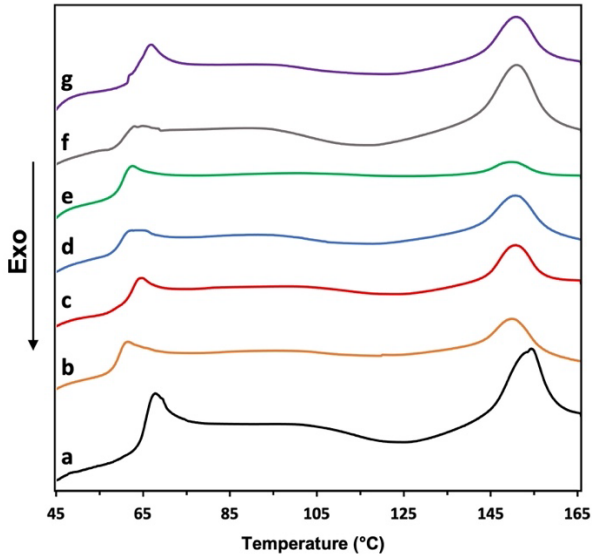


**Figure 5.** DSC exotherms of binary and ternary blends obtained from the first heating cycle: (a) neat PLA; (b) 20-PF; (c) 20-HPF; (d) 20-PFGMA; (e) 20-PFMAA; (f) 10-PFGMA/10-PFMAA; and (g) 15-PFGMA/15-PFMAA. Samples were taken from the fractured impact bars.

The $T_g$s of the binary and ternary blends are shown in Table 3 (see Supplementary Information, Figure S5 for curves). Each blend exhibits two $T_g$s which correspond to the $T_g$s of the individual components in the blends, with the values shifting slightly closer to one another owing to the interactions between the *Far* phase and the PLA phase. The two ternary blends exhibited the highest upward shift of the first $T_g$, and downward shift of the second $T_g$, which indicates their partial miscibility with PLA. The thermal stability of the blends was also evaluated with TGA, with all blends exhibiting equal or higher $T_{d,10\%}$ values than PLA (see Supplementary Information, Figure S4 for curves).

**Table 3.** Thermal properties of binary and ternary blends.

| **Blend** | $T_m$ (°C)[a] | $T_{cc}$ (°C)[a] | $X_c$ (%) | $T_{g1}^{(DSC)}$ (°C)[b] | $T_{g2}^{(DSC)}$ (°C)[b] | $T_g^{(DMTA)}$ (°C)[c] | $T_{d,10\%}$ (°C)[d] |
|---|---|---|---|---|---|---|---|
| PLA | 153.9 | 125.2 | 5.9 | - | 59.6 | 67.0 | 328 |
| 20-PF | 149.8 | 119.4 | 4.8 | -69.4 | 57.9 | 65.4 | 326 |
| 20-HPF | 150.5 | 124.3 | 1.4 | -58.1 | 58.4 | 66.1 | 339 |
| 20-PFGMA | 150.2 | 119.4 | 3.3 | -68.0 | 58.4 | 64.0 | 336 |
| 20-PFMA | 149.9 | 127.0 | 3.3 | -68.6 | 57.3 | 65.8 | 327 |
| 10-PFGMA/10-PFMAA | 150.4 | 115.1 | 7.9 | -67.1 | 57.8 | 65.9 | 339 |
| 15-PFGMA/15-PFMAA | 150.3 | 119.7 | 5.9 | -66.5 | 58.3 | 65.4 | 342 |

[a] Measured from the first heating cycle of DSC exotherm
[b] Measured from the second heating cycle of DSC exotherm
[c] Measured from peak of tan$\delta$ curve with DMTA
[d] Onset temperature at 10% mass loss measured with TGA

## Blend Miscibility

The miscibility between components in polymer blends has significant influence on both the phase behaviour and resultant mechanical properties of the processed materials. Therefore, dynamic mechanical thermal analysis (DTMA) was used to evaluate the miscibility between the components in the prepared blends. In Figures 6a and b, the storage modulus (*G'*) and tanδ curves of neat PLA along with the binary and ternary blends are shown. At room temperature, the *G'* of the blends decreases relative to PLA owing to the presence of the soft, rubbery *Far*-based components. Glass transitions were observed between 55-65 °C for the binary and ternary blends, followed by a sharp decrease in *G'* before reaching the rubbery plateau region. In all cases, cold crystallization peaks were clearly observed, with all blends exhibiting a shift to a higher $T_{cc}$ (between 112-120 °C) relative to neat PLA ($T_{cc}$ ~100 °C).

As shown in Figure 6b, the tanδ peak for neat PLA was observed at 67 °C which corresponded to its $T_g$. For the binary and ternary blends a slight decrease in temperature was observed for their tanδ peaks relative to PLA, with the largest shift obtained for the 20-PFGMA binary blend (64 °C). These shifts to slightly lower temperatures were in agreement with our DSC results and are due to the presence of the rubbery *Far* components in the blends which exhibit $T_g$ values ranging

from -71.8 to -58.5 °C. The more pronounced shift of the tanδ peak for the 20-PFMGA blend indicated a higher degree of miscibility between the two phases in the blend owing to the presence of the GMA functional groups which are known to enhance compatibility in PLA rubber toughened blends.[59]

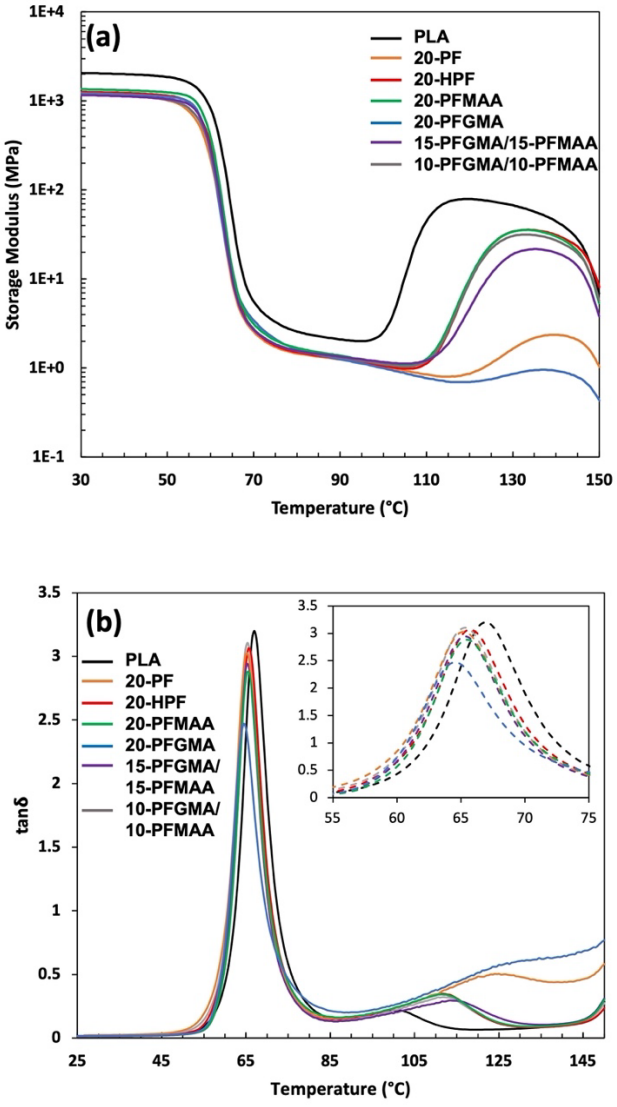


**Figure 6.** DMTA traces of neat PLA, binary, and ternary blends: (a) Storage modulus (*G'*) vs temperature; (b) tanδ vs temperature.

## Blend Morphology

In Figure 7, the cryo-fractured and cryo-microtomed surfaces of the binary and ternary blends is shown, while the weighted-average particle diameters ($d_w$) are summarized in Table 4. In the case of the four binary blends, large dispersed phase droplets are clearly visible, with $d_w$ values ranging from 2.9 to 4.3 μm, and polydispersities between 1.8 and 2.5. In immiscible binary systems, this morphology of discrete dispersion of the minor phase with a higher polydispersity is commonly observed,[60] and helps to explain the poor mechanical properties obtained with these blends as the large droplets facilitated fracture during testing.

Conversely, the surface morphologies of the two ternary blends revealed much finer droplet sizes, with more sub-micron particles being observed. In the 10-PFGMA/10-PFMAA blend, the $d_w$ decreased to 1.3 μm, while the $d_w$ of the 15/15 blend further decreased to 1.1 μm. As a result of the interfacial compatibilization reaction, the formed graft copolymers stabilized the interface between PLA and the *Far* phases. This prevented dispersed phase coalescence into larger droplets while retaining relatively monodisperse particle sizes.[51]

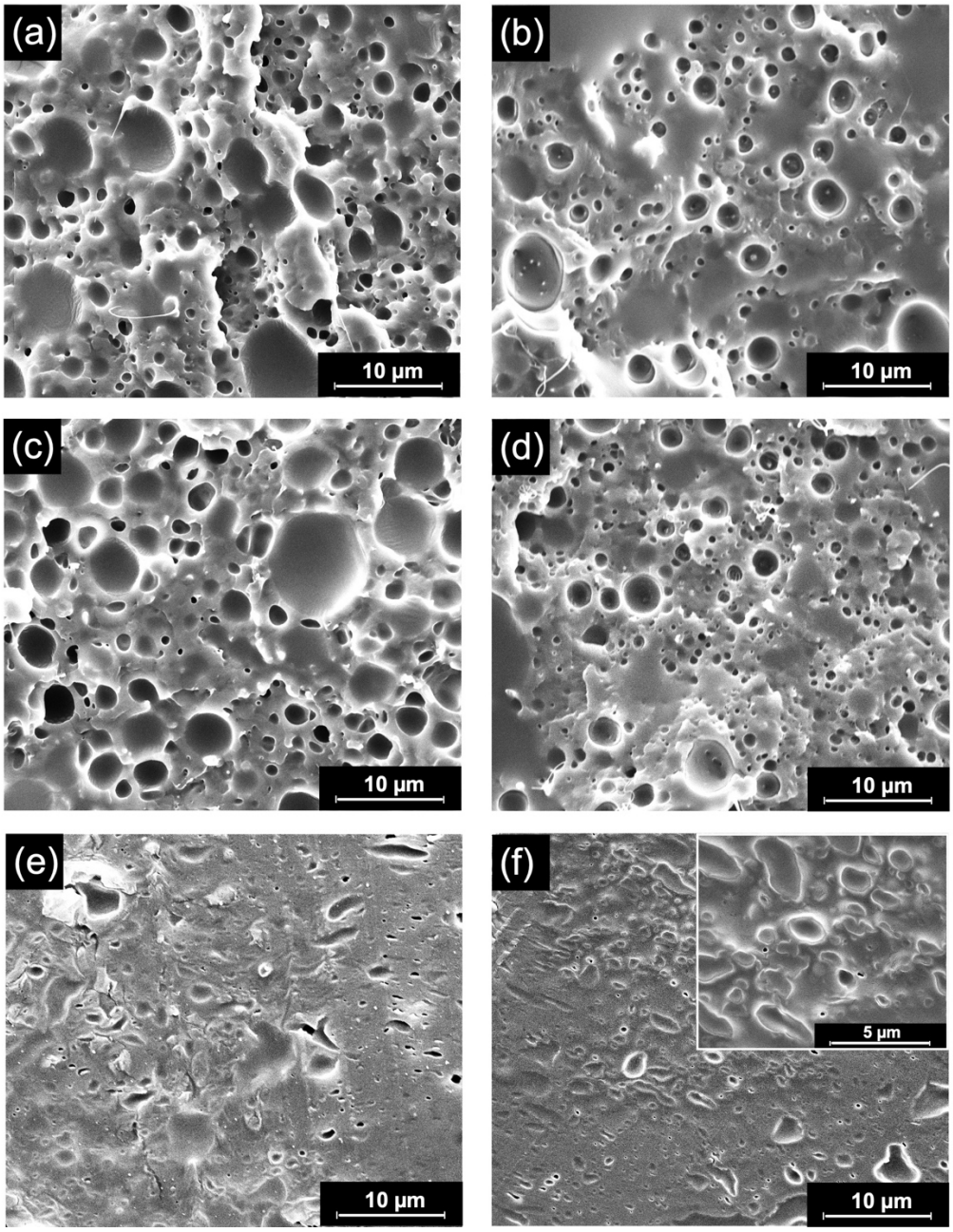


**Figure 7.** Cryo-fractured (a-d) and cryo-microtomed (e,f) SEM images of binary and ternary blends: (a) 20-PF; (b) 20-HPF; (c) 20-PFGMA; (d) 20-PFMAA; (e) 10-PFGMA/10-PFMAA; and (f) 15-PFGMA/15-PFMAA (inset shows higher magnification).

To evaluate the stability of the blends, selected samples were thermally annealed at 100 °C for 8 hours under vacuum. After annealing, the 20-PFGMA and 20-PFMAA binary blends resulted in relatively coarse morphologies, with larger droplets being observed ~ 3-4 µm. In both cases, the $d_w$ and the polydispersity increased after annealing, which suggested that these blends were unstable (Table 4 and Figure S6). However, the morphology of the ternary blends did not

significantly differ after thermal annealing, as the $d_w$ and the polydispersity remained relatively unchanged. These results suggest that the acid-epoxy/hydroxyl-epoxy compatibilization reaction occurring in the ternary blends was more effective at producing stable morphologies with finer particle size than the non-reactive binary systems.

**Table 4.** Particle diameter measurements of binary and ternary blends.

| Blend | $d_w$ (μm) | Polydispersity ($d_w/d_n$) |
|---|---|---|
| 20-PF | 3.1 | 2.3 |
| 20-HPF | 2.9 | 2.5 |
| 20-PFGMA | 4.3 (8.1)[a] | 1.9 (2.8) [a] |
| 20-PFMAA | 3.2 (5.8)[a] | 1.8 (2.5)[a] |
| 10-PFGMA/10-PFMAA | 1.3 (1.4)[a] | 1.1 (1.2)[a] |
| 15-PFGMA/15-PFMAA | 1.1 (1.1)[a] | 1.1 (1.1)[a] |

[a] After thermal annealing at 100 °C for 8 hours.

## Surface Morphology of Fractured Impact Bars

The surface morphology of fractured impact bars was evaluated with SEM to gain insights into the mechanism behind the enhanced impact toughness observed for the ternary blends (Figure 8). Neat PLA underwent typical brittle fracture to reveal a smooth and featureless fracture surface,[61] while the 20-PFMAA and 20-PFGMA binary blends began to exhibit fracture lines and ridges in close proximity to the dispersed rubber phase droplets (Figure 8a and b). In both cases, phase separation is clear, indicating poor interfacial adhesion between PLA and the *Far* phases which was reflected in the marginal improvements in impact strength obtained with these two binary blends.

In contrast to the binary blends, the interface between the *Far* phases and PLA is harder to discern in the ternary blends, demonstrating the enhanced compatibility arising from the occurrence of cross-linking interfacial reactions (Figures 8c and d). Moreover, the fracture surfaces contain several long fibril strands which indicate plastic deformation and ductile fracture during impact, with more fibrils present in the 15/15 blend. In both cases, significant plastic deformation adjacent to the dispersed phase was evident which implies that shear yielding of the PLA matrix has taken place and helps to explain the significant improvement in impact strength observed with these

blends.[62] This type of mechanism in which strong interfacial adhesion leading to plastic deformation and shear yielding is one which has been commonly observed in other multiphase blends.[49, 63]

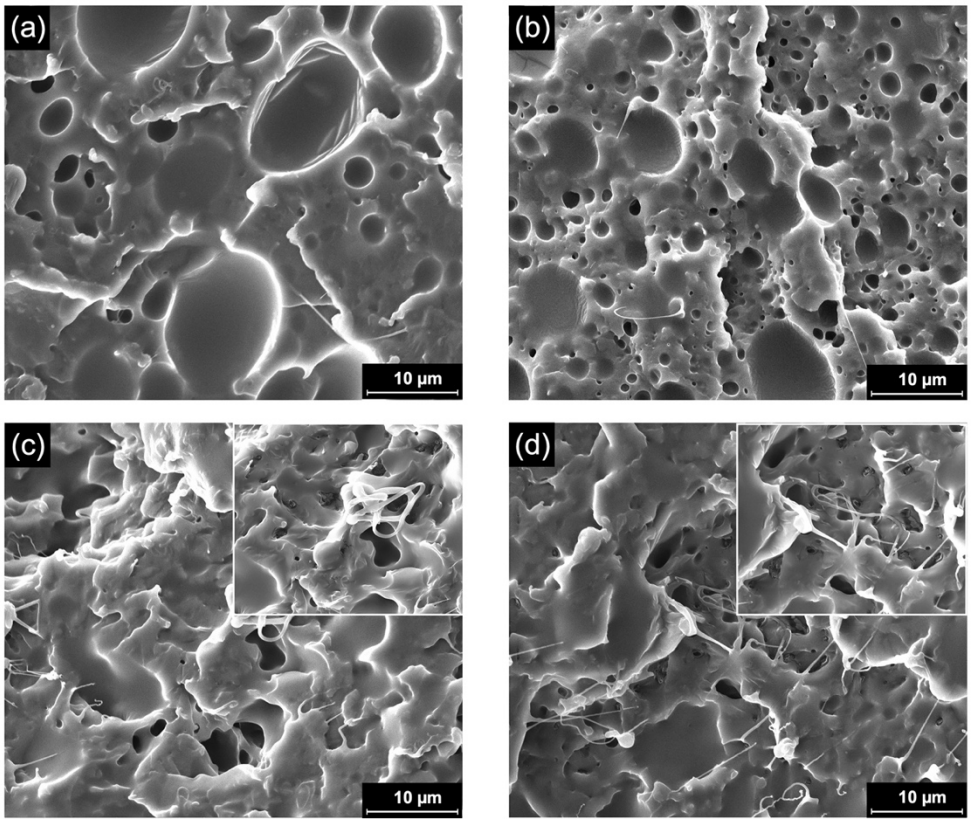


**Figure 8.** SEM images of impact fracture surface adjacent to the notch of selected blends: (a) 20-PFMA; (b) 20-PFGMA; (c) 10-PFGMA/10-PFMAA; and (d) 15-PFGMA/15-PFMAA (2500x magnification, insets show 5000 × magnification of fibrils).

## Reactive Compatibilization Mechanism

During mixing, the change in torque was measured over time using the Haake internal batch mixer to monitor the evolution of potential interfacial compatibilization reactions occurring. In general, a higher torque output is correlated with an increase in blend viscosity which can signify copolymer formation.[47] Figure 9(a) shows the torque outputs of the four binary blends which follow similar profiles throughout mixing. Initially, there is a sharp increase in torque as the blends melt inside the chamber and then reach a steady state region after ~ 100 seconds as the torque

profiles become flat over time. While the steady state torque profiles illustrate that the blends are stable rheologically under these mixing parameters, they suggest that little to no chemical reaction occurs between the epoxy groups on PFGMA and the acid/hydroxyl groups on PLA as no change in torque was observed.

Previous work has shown that the epoxy-acid/epoxy-hydroxyl interfacial reaction can be promoted through the addition of a catalyst during blending, or through increasing the mixing temperature above 210 °C.[12, 46-48, 57, 58] Alternatively, the use of multicomponent polymer blends have been successfully employed to promote interfacial compatibilization through dynamic vulcanization in which elastomers are selectively vulcanized during mixing with PLA to generate a cross-linked network.[57, 64] This strategy, when used in conjunction with elevated mixing temperatures, has proven useful in the past to promote epoxy-acid interfacial compatibilization reactions using zinc catalysis to generate toughened PLA blends.[58] Therefore, we postulated whether a ternary system comprised of PLA, PFGMA, and PFMAA could undergo a similar transformation catalyzed through intermolecular hydrogen bonding to promote interfacial reactivity.

In the case of our ternary systems, a large increase in torque was observed after 150 (15-PFGMA/15-PFMAA) and 200 (10-PFGMA/10-PFMAA) seconds of mixing time, as shown in Figure 9(b). This large and rapid increase in torque was attributed to cross-linking reactions occurring between the epoxy groups on PFGMA, the acid groups on PFMAA, and the acid/hydroxyl groups on PLA. Akin to the work by Liu *et al.,*[57] the generation of a cross-linked elastomeric network in our system led to an increase in blend viscosity and torque output over the course of the reaction. The manifestation of the interfacial compatibilization reactions were substantiated by the reduction in particle size of the dispersed phase coupled with significant improvements in impact strength.

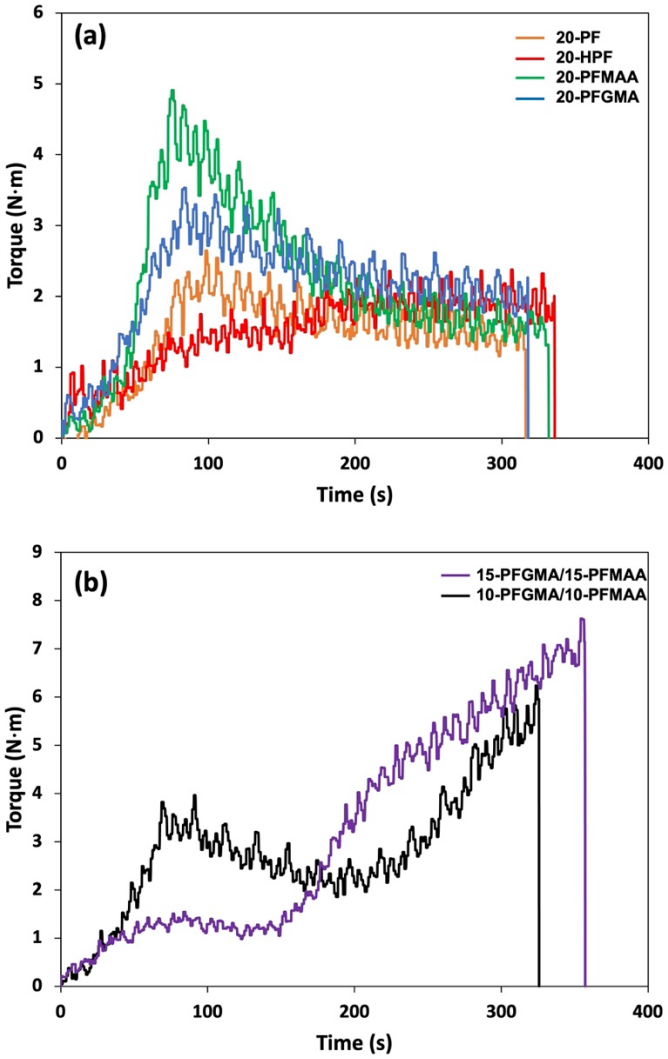


**Figure 9.** Torque vs time plots obtained from the internal batch mixer for (a) binary blends and (b) ternary blends.

To further investigate the cross-linking reaction and identify the chemical structure of the newly formed species, FTIR was employed. Figure 10 shows the FTIR absorbance spectra of the three neat homopolymers (PLA, PFGMA, PFMAA) and the cross-linked fractions from the two ternary blends. The ternary blends were etched with chloroform to dissolve PLA, PFGMA, and PFMAA, while the insoluble portion was collected and dried under vacuum prior to analysis (see Supplementary Information, Figure S7 for the visual appearance). PLA exhibits strong stretching vibration peaks at 1747 $cm^{-1}$ and 1080 $cm^{-1}$ which correspond to the C=O and C-O groups in the backbone, respectively.[65] PFGMA shows strong -$CH_3$ stretching vibration at 2917 $cm^{-1}$, C=O

stretching at 1733 $cm^{-1}$, and -$CH_3$ bending at 1447 $cm^{-1}$ and 1376 $cm^{-1}$. In the case of PFMAA, the majority of the free carboxylic acid groups existed as intermolecular dimers which exhibit a stretching vibration at 1698 $cm^{-1}$.[66]

For the two ternary blends, the insoluble cross-linked portions showed a strong, broadened peak at 1753 $cm^{-1}$ which was attributed to the carbonyl group from the PLA backbone, a broad shoulder peak at 1698 $cm^{-1}$ attributed to the carboxylic acid dimer from PFMAA, as well as a weak alkene stretching peak present at 1667 $cm^{-1}$ which can be associated with the presence of both PFMAA and PFGMA. Furthermore, prominent -$CH_3$ stretching vibrations are evident in both ternary blend samples and are characteristic of the *Far* polymers. Finally, the broad peak ranging from 3200-3600 $cm^{-1}$ indicates the presence of both free and intermolecularly bonded hydroxyl groups[67] resulting from the ring-opening of the epoxy groups of PFGMA through nucleophilic attack of acid/hydroxyl groups. While present in both ternary blends, the signal intensity appears stronger in the 15-PFGMA/15-PFMAA blend, indicating a higher degree of epoxy-acid/epoxy-hydroxyl reactions occurring and helps to explain the enhanced impact strength observed with this blend.

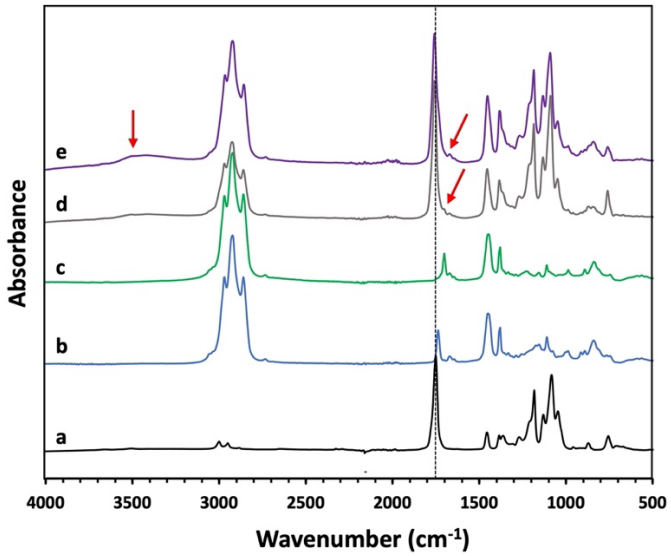


**Figure 10.** FTIR absorption spectra of homopolymers and cross-linked portions from ternary blends: (a) neat PLA; (b) neat PFGMA; (c) neat PFMAA; (d) $CHCl_3$-extracted portion of 10-PFGMA/10-PFMAA; and (e) $CHCl_3$-extracted portion of 15-PFGMA/15-PFMAA.

A proposed reaction mechanism is presented in Scheme 1 to account for the enhanced material properties obtained with the ternary blends as well as the formation of the cross-linked species.

During the initial stages of mixing, PFGMA and PFMAA will preferentially coalesce with one another inside of the PLA matrix owing to their hydrophobic *Far* chains, with the polar GMA and MA functional groups being positioned on the surface of the droplets. At this interface, the oxygen atom in the epoxide acts as a hydrogen bond acceptor from the neighbouring carboxylic acid donor present in PFMAA; effectively polarizing the carbon-oxygen bond to increase the electrophilicity of the adjacent methylene. This is followed by nucleophilic attack by either the hydroxyl and/or acid group of PLA, or by the acid functionalized PFMAA to generate the corresponding cross-linked polymer network. Previous mechanistic studies with small molecules have shown the effectiveness of hydrogen bonding catalysis on epoxide ring opening,[68-70] although this usually is facilitated by the addition of a phenol-based catalyst. Here, we show that this transformation can also proceed using carboxylic acid as the hydrogen bonding donor to catalyze the interfacial compatibilization reaction between two immiscible phases in the melt.

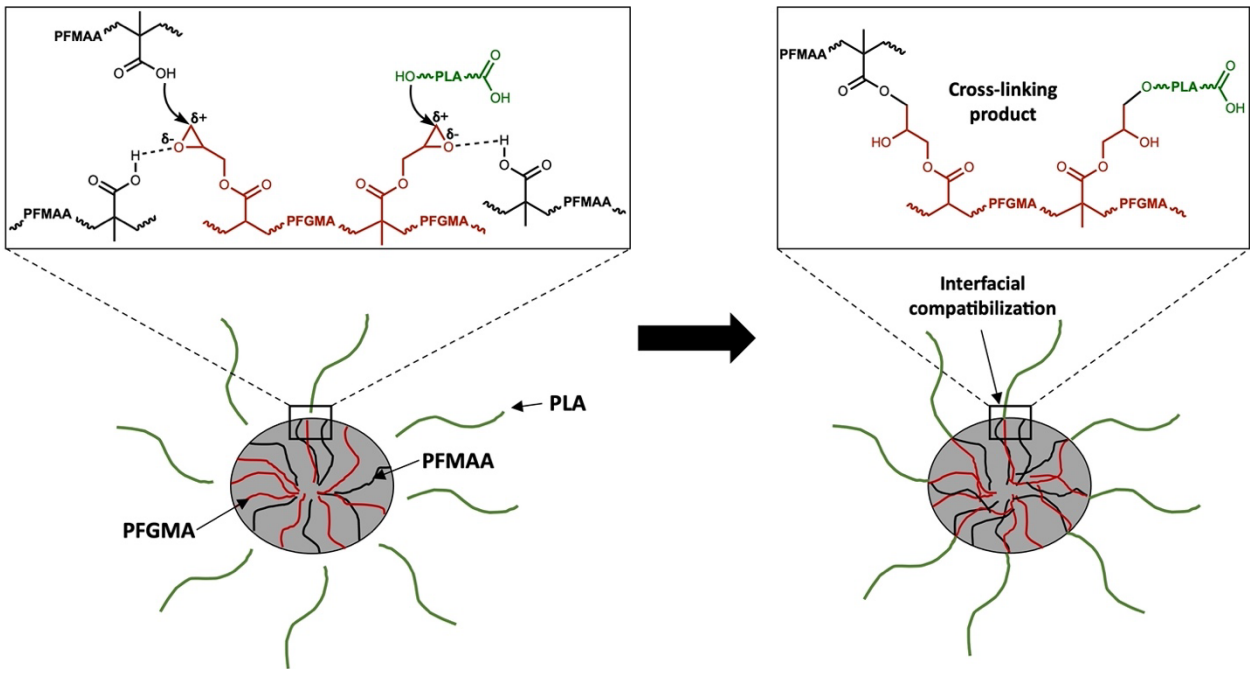


**Scheme 1.** Proposed interfacial compatibilization reaction mechanism during blending leading to formation of cross-linked product with the ternary blends.

## Conclusions

The bio-based monomer *Far,* was used as a building block for the design of functionalized elastomeric additives which were then evaluated as rubber toughening agents for PLA. Toughened ternary blends consisting of PLA/PFGMA/PFMAA exhibited an impact strength of 366 J/m (16-fold greater than PLA) which were achieved through interfacial compatibilization reactions to generate a cross-linked polymer network inside of the PLA matrix. The chemical structure of the cross-linked network was elucidated with FTIR and established the occurrence of epoxy-acid/epoxy-hydroxyl reactions between all three components in the blend. The morphological analysis of the blends showed a significant reduction in the particle size of the dispersed phase from 4.3 μm in the binary blend, to 1.1 μm in the ternary blend. Finally, improved interfacial adhesion in conjunction with substantial shear yielding of the matrix were determined as the underlying mechanism responsible for enhanced impact strength in the ternary systems. This work demonstrates the applicability of bio-based *Far* polymers as rubber toughening agents to produce sustainably sourced toughened PLA blends.

## Funding

This research was generously supported by the Natural Sciences and Engineering Research Council of Canada (Collaborative Research and Development Grants, CRDPJ 543853-2019 and Discovery Grants Program, RGPIN 05948-2019, RGPIN 06161-2018, 2016-03792) and the James McGill Chair program of McGill University. Student funding was provided by the Fonds de Recherche du Québec - Nature et Technologie (FRQNT), which granted Matthew W. Halloran a Doctoral Scholarship administered under the B2X program.

## Supporting Information

Supporting Information is available …

## Acknowledgements

The authors thank the McGill Chemistry Characterization facility for use of their facility, whose operations are supported by the Quebec Center for Advanced Materials (QCAM). They also acknowledge and thank the Department of Chemical Engineering at Polytechnique Montréal for the use of their facility to perform Izod impact testing. They would also like to thank Dr. Georges

Younes for sharing his rheology expertise, and Dr. Sharmaine Luk for her helpful discussions relating to the synthesis. The authors also thank Derek McPhee from Amyris for facilitating the acquisition of the farnesene used in this study. Finally, they would like to acknowledge and thank the McGill Facility for Electron Microscopy Research (FEMR) for use of their equipment and sample preparation.

# References

1. Sangeetha, V. H.; Deka, H.; Varghese, T. O.; Nayak, S. K., State of the art and future prospectives of poly(lactic acid) based blends and composites. *Polym. Compos.* **2018,** *39* (1), 81-101.
2. Reichert, C. L.; Bugnicourt, E.; Coltelli, M. B.; Cinelli, P.; Lazzeri, A.; Canesi, I.; Braca, F.; Martinez, B. M.; Alonso, R.; Agostinis, L.; Verstichel, S.; Six, L.; De Mets, S.; Gomez, E. C.; Issbrucker, C.; Geerinck, R.; Nettleton, D. F.; Campos, I.; Sauter, E.; Pieczyk, P.; Schmid, M., Bio-Based Packaging: Materials, Modifications, Industrial Applications and Sustainability. *Polymers* **2020,** *12* (7).
3. da Silva, D.; Kaduri, M.; Poley, M.; Adir, O.; Krinsky, N.; Shainsky-Roitman, J.; Schroeder, A., Biocompatibility, biodegradation and excretion of polylactic acid (PLA) in medical implants and theranostic systems. *Chem. Eng. J.* **2018,** *340*, 9-14.
4. Singhvi, M. S.; Zinjarde, S. S.; Gokhale, D. V., Polylactic acid: synthesis and biomedical applications. *J. Appl. Microbiol.* **2019,** *127* (6), 1612-1626.
5. Farah, S.; Anderson, D. G.; Langer, R., Physical and mechanical properties of PLA, and their functions in widespread applications — A comprehensive review. *Adv. Drug Deliv. Rev.* **2016,** *107*, 367-392.
6. Halloran, M. W.; Danielczak, L.; Nicell, J. A.; Leask, R. L.; Marić, M., Highly Flexible Polylactide Food Packaging Plasticized with Nontoxic, Biosourced Glycerol Plasticizers. *ACS Appl. Polym. Mater.* **2022,** *4* (5), 3608-3617.
7. Hamad, K.; Kaseem, M.; Ayyoob, M.; Joo, J.; Deri, F., Polylactic acid blends: The future of green, light and tough. *Prog. Polym. Sci.* **2018,** *85*, 83-127.
8. Liu, H.; Zhang, J., Research progress in toughening modification of poly(lactic acid). *J. Polym. Sci. B Polym. Phys.* **2011,** *49* (15), 1051-1083.
9. Zhao, X.; Hu, H.; Wang, X.; Yu, X.; Zhou, W.; Peng, S., Super tough poly(lactic acid) blends: a comprehensive review. *RSC Advances* **2020,** *10* (22), 13316-13368.
10. Krishnan, S.; Pandey, P.; Mohanty, S.; Nayak, S. K., Toughening of Polylactic Acid: An Overview of Research Progress. *Polym. Plast. Technol. Eng.* **2016,** *55* (15), 1623-1652.
11. Alias, N. F.; Ismail, H., An overview of toughening polylactic acid by an elastomer. *Polym. Plast. Technol. Mat.* **2019,** *58* (13), 1399-1422.
12. Thurber, C. M.; Xu, Y.; Myers, J. C.; Lodge, T. P.; Macosko, C. W., Accelerating Reactive Compatibilization of PE/PLA Blends by an Interfacially Localized Catalyst. *ACS Macro Lett.* **2015,** *4* (1), 30-33.

13. Rigoussen, A.; Verge, P.; Raquez, J.-M.; Habibi, Y.; Dubois, P., In-depth investigation on the effect and role of cardanol in the compatibilization of PLA/ABS immiscible blends by reactive extrusion. *Eur. Polym. J.* **2017,** *93*, 272-283.
14. Akos, N. I.; Wahit, M. U.; Mohamed, R.; Yussuf, A. A., Comparative studies of mechanical properties of poly(ε-caprolactone) and poly(lactic acid) blends reinforced with natural fibers. *Compos. Interfaces* **2013,** *20* (7), 459-467.
15. Wu, F.; Misra, M.; Mohanty, A. K., Tailoring the toughness of sustainable polymer blends from biodegradable plastics via morphology transition observed by atomic force microscopy. *Polym. Degrad. Stab.* **2020,** *173*, 109066.
16. Yuryev, Y.; Mohanty, A. K.; Misra, M., Novel super-toughened bio-based blend from polycarbonate and poly(lactic acid) for durable applications. *RSC Advances* **2016,** *6* (107), 105094-105104.
17. Oyama, H. T., Super-tough poly(lactic acid) materials: Reactive blending with ethylene copolymer. *Polymer* **2009,** *50* (3), 747-751.
18. Wang, M.; Wu, Y.; Li, Y.-D.; Zeng, J.-B., Progress in Toughening Poly(Lactic Acid) with Renewable Polymers. *Polym. Rev.* **2017,** *57* (4), 557-593.
19. Dong, W.; Cao, X.; Li, Y., High-performance biosourced poly(lactic acid)/polyamide 11 blends with controlled salami structure. *Polym. Int.* **2014,** *63* (6), 1094-1100.
20. Rasselet, D.; Caro-Bretelle, A.-S.; Taguet, A.; Lopez-Cuesta, J.-M., Reactive Compatibilization of PLA/PA11 Blends and Their Application in Additive Manufacturing. *Materials (Basel)* **2019,** *12* (3), 485.
21. Yeo, J. C. C.; Muiruri, J. K.; Tan, B. H.; Thitsartarn, W.; Kong, J.; Zhang, X.; Li, Z.; He, C., Biodegradable PHB-Rubber Copolymer Toughened PLA Green Composites with Ultrahigh Extensibility. *ACS Sustain. Chem. Eng.* **2018,** *6* (11), 15517-15527.
22. Thakur, S.; Cisneros-Lopez, E. O.; Pin, J.-M.; Misra, M.; Mohanty, A. K., Green Toughness Modifier from Downstream Corn Oil in Improving Poly(lactic acid) Performance. *ACS Appl. Polym. Mater.* **2019,** *1* (12), 3396-3406.
23. Mauck, S. C.; Wang, S.; Ding, W.; Rohde, B. J.; Fortune, C. K.; Yang, G.; Ahn, S.-K.; Robertson, M. L., Biorenewable Tough Blends of Polylactide and Acrylated Epoxidized Soybean Oil Compatibilized by a Polylactide Star Polymer. *Macromolecules* **2016,** *49* (5), 1605-1615.
24. Muiruri, J. K.; Liu, S.; Teo, W. S.; Kong, J.; He, C., Highly Biodegradable and Tough Polylactic Acid–Cellulose Nanocrystal Composite. *ACS Sustain. Chem. Eng.* **2017,** *5* (5), 3929-3937.
25. Yang, W.; Weng, Y.; Puglia, D.; Qi, G.; Dong, W.; Kenny, J. M.; Ma, P., Poly(lactic acid)/lignin films with enhanced toughness and anti-oxidation performance for active food packaging. *Int. J. Biol. Macromol.* **2020,** *144*, 102-110.
26. Abdelwahab, M. A.; Jacob, S.; Misra, M.; Mohanty, A. K., Super-tough sustainable biobased composites from polylactide bioplastic and lignin for bio-elastomer application. *Polymer* **2021,** *212*, 123153.
27. Luk, S. B.; Azevedo, L. A.; Maric, M., Reversible deactivation radical polymerization of bio-based dienes. *React. Funct. Polym.* **2021,** *162*, 104871.
28. Hulnik, M. I.; Vasilenko, I. V.; Radchenko, A. V.; Peruch, F.; Ganachaud, F.; Kostjuk, S. V., Aqueous cationic homo- and co-polymerizations of β-myrcene and styrene: a green route toward terpene-based rubbery polymers. *Polym. Chem-Uk* **2018,** *9* (48), 5690-5700.

29. Yoo, T.; Henning, S. K., Synthesis and characterization of farnesene-based polymers. *Rubber Chem. Technol.* **2017,** *90* (2), 308-324.
30. Bolton, J. M.; Hillmyer, M. A.; Hoye, T. R., Sustainable Thermoplastic Elastomers from Terpene-Derived Monomers. *ACS Macro Lett.* **2014,** *3* (8), 717-720.
31. Dalsin, S. J.; Hillmyer, M. A.; Bates, F. S., Linear Rheology of Polyolefin-Based Bottlebrush Polymers. *Macromolecules* **2015,** *48* (13), 4680-4691.
32. Wahlen, C.; Blankenburg, J.; von Tiedemann, P.; Ewald, J.; Sajkiewicz, P.; Müller, A. H. E.; Floudas, G.; Frey, H., Tapered Multiblock Copolymers Based on Farnesene and Styrene: Impact of Biobased Polydiene Architectures on Material Properties. *Macromolecules* **2020,** *53* (23), 10397-10408.
33. Sarkar, P.; Bhowmick, A. K., Synthesis, characterization and properties of a bio-based elastomer: polymyrcene. *RSC Advances* **2014,** *4* (106), 61343-61354.
34. Rude, M. A.; Schirmer, A., New microbial fuels: a biotech perspective. *Curr. Opin. Microbiol.* **2009,** *12* (3), 274-281.
35. Cawse, J. L.; Stanford, J. L.; Still, R. H., Polymers from renewable sources: 5. Myrcene-based polyols as rubber-toughening agents in glassy polyurethanes. *Polymer* **1987,** *28* (3), 368-374.
36. Zhou, C.; Wei, Z.; Jin, C.; Wang, Y.; Yu, Y.; Leng, X.; Li, Y., Fully biobased thermoplastic elastomers: Synthesis of highly branched linear comb poly(β-myrcene)-graft-poly(l-lactide) copolymers with tunable mechanical properties. *Polymer* **2018,** *138*, 57-64.
37. Luk, S. B.; Métafiot, A.; Morize, J.; Edeh, E.; Marić, M., Hydrogenation of poly(myrcene) and poly(farnesene) using diimide reduction at ambient pressure. *J. Polym. Sci.* **2021,** *59* (19), 2140-2153.
38. Marić, M.; Ashurov, N.; Macosko, C. W., Reactive blending of poly (dimethylsiloxane) with nylon 6 and poly (styrene):Effect of reactivity on morphology. *Polym. Eng. Sci.* **2001,** *41* (4), 631-642.
39. Nerkar, M.; Ramsay, J. A.; Ramsay, B. A.; Kontopoulou, M., Dramatic Improvements in Strain Hardening and Crystallization Kinetics of PLA by Simple Reactive Modification in the Melt State. *Macromol. Mater. Eng.* **2014,** *299* (12), 1419-1424.
40. Fetters, L. J.; Lohse, D. J.; Richter, D.; Witten, T. A.; Zirkel, A., Connection between Polymer Molecular Weight, Density, Chain Dimensions, and Melt Viscoelastic Properties. *Macromolecules* **1994,** *27* (17), 4639-4647.
41. Iacob, C.; Yoo, T.; Runt, J., Molecular Dynamics of Polyfarnesene. *Macromolecules* **2018,** *51* (13), 4917-4922.
42. Sahu, P.; Bhowmick, A. K., Redox Emulsion Polymerization of Terpenes: Mapping the Effect of the System, Structure, and Reactivity. *Ind. Eng. Chem. Res.* **2019,** *58* (46), 20946-20960.
43. Luk, S. B.; Maríc, M., Polymerization of Biobased Farnesene in Miniemulsions by Nitroxide-Mediated Polymerization. *ACS Omega* **2021,** *6* (7), 4939-4949.
44. Luk, S. B.; Marić, M., Nitroxide-Mediated Polymerization of Bio-Based Farnesene with a Functionalized Methacrylate. *Macromol. React. Eng.* **2019,** *13* (3), 1800080.
45. Bai, H.; Bai, D.; Xiu, H.; Liu, H.; Zhang, Q.; Wang, K.; Deng, H.; Chen, F.; Fu, Q.; Chiu, F.-C., Towards high-performance poly(l-lactide)/elastomer blends with tunable interfacial adhesion and matrix crystallization via constructing stereocomplex crystallites at the interface. *RSC Advances* **2014,** *4* (90), 49374-49385.

46. Feng, Y.; Zhao, G.; Yin, J.; Jiang, W., Reactive compatibilization of high-impact poly(lactic acid)/ethylene copolymer blends catalyzed by N,N-dimethylstearylamine. *Polym. Int.* **2014,** *63* (7), 1263-1269.
47. Thurber, C.; Gu, L.; Myers, J. C.; Lodge, T. P.; Macosko, C. W., Toughening polylactide with a catalyzed epoxy-acid interfacial reaction. *Polym. Eng. Sci.* **2018,** *58* (1), 28-36.
48. Yuryev, Y.; Mohanty, A. K.; Misra, M., A New Approach to Supertough Poly(lactic acid): A High Temperature Reactive Blending. *Macromol. Mater. Eng.* **2016,** *301* (12), 1443-1453.
49. Zhang, K.; Nagarajan, V.; Misra, M.; Mohanty, A. K., Supertoughened Renewable PLA Reactive Multiphase Blends System: Phase Morphology and Performance. *ACS Appl. Mater. Inter.* **2014,** *6* (15), 12436-12448.
50. Favis, B. D.; Chalifoux, J. P., The effect of viscosity ratio on the morphology of polypropylene/polycarbonate blends during processing. *Polym. Eng. Sci.* **1987,** *27* (21), 1591-1600.
51. Sundararaj, U.; Macosko, C. W., Drop Breakup and Coalescence in Polymer Blends: The Effects of Concentration and Compatibilization. *Macromolecules* **1995,** *28* (8), 2647-2657.
52. Oxby, K. J.; Marić, M., Compatibilization of Poly(styrene-acrylonitrile) (SAN)/Poly(ethylene) Blends via Amine Functionalization of SAN Chain Ends. *Macromol. React. Eng.* **2014,** *8* (2), 160-169.
53. Chang, K.; Robertson, M. L.; Hillmyer, M. A., Phase Inversion in Polylactide/Soybean Oil Blends Compatibilized by Poly(isoprene-b-lactide) Block Copolymers. *ACS Appl. Mater. Inter.* **2009,** *1* (10), 2390-2399.
54. Han, L.; Han, C.; Dong, L., Morphology and properties of the biosourced poly(lactic acid)/poly(ethylene oxide-b-amide-12) blends. *Polym. Compos.* **2013,** *34* (1), 122-130.
55. Kowalczyk, M.; Piorkowska, E., Mechanisms of plastic deformation in biodegradable polylactide/poly(1,4-cis-isoprene) blends. *J. Appl. Polym. Sci.* **2012,** *124* (6), 4579-4589.
56. Bhardwaj, R.; Mohanty, A. K., Modification of Brittle Polylactide by Novel Hyperbranched Polymer-Based Nanostructures. *Biomacromolecules* **2007,** *8* (8), 2476-2484.
57. Liu, H.; Chen, F.; Liu, B.; Estep, G.; Zhang, J., Super Toughened Poly(lactic acid) Ternary Blends by Simultaneous Dynamic Vulcanization and Interfacial Compatibilization. *Macromolecules* **2010,** *43* (14), 6058-6066.
58. Liu, H.; Guo, L.; Guo, X.; Zhang, J., Effects of reactive blending temperature on impact toughness of poly(lactic acid) ternary blends. *Polymer* **2012,** *53* (2), 272-276.
59. Nagarajan, V.; Mohanty, A. K.; Misra, M., Perspective on Polylactic Acid (PLA) based Sustainable Materials for Durable Applications: Focus on Toughness and Heat Resistance. *ACS Sustain. Chem. Eng.* **2016,** *4* (6), 2899-2916.
60. Ougizawa, T.; Inoue, T., Morphology of Polymer Blends. In *Polymer Blends Handbook*, Utracki, L. A.; Wilkie, C. A., Eds. Springer Netherlands: Dordrecht, 2014; pp 875-918.
61. Zhang, K.; Mohanty, A. K.; Misra, M., Fully Biodegradable and Biorenewable Ternary Blends from Polylactide, Poly(3-hydroxybutyrate-co-hydroxyvalerate) and Poly(butylene succinate) with Balanced Properties. *ACS Appl. Mater. Inter.* **2012,** *4* (6), 3091-3101.
62. Li, Y.; Shimizu, H., Toughening of Polylactide by Melt Blending with a Biodegradable Poly(ether)urethane Elastomer. *Macromol. Biosci.* **2007,** *7* (7), 921-928.
63. Wu, N.; Zhang, H., Mechanical properties and phase morphology of super-tough PLA/PBAT/EMA-GMA multicomponent blends. *Mater. Lett.* **2017,** *192*, 17-20.

64. Liu, H.; Song, W.; Chen, F.; Guo, L.; Zhang, J., Interaction of Microstructure and Interfacial Adhesion on Impact Performance of Polylactide (PLA) Ternary Blends. *Macromolecules* **2011,** *44* (6), 1513-1522.
65. Chieng, B. W.; Ibrahim, N. A.; Yunus, W. M. Z. W.; Hussein, M. Z., Poly(lactic acid)/Poly(ethylene glycol) Polymer Nanocomposites: Effects of Graphene Nanoplatelets. *Polymers* **2014,** *6* (1), 93-104.
66. Coleman, M. M.; Lee, J. Y.; Painter, P. C., Acid salts and the structure of ionomers. *Macromolecules* **1990,** *23* (8), 2339-2345.
67. Moskala, E. J.; Howe, S. E.; Painter, P. C.; Coleman, M. M., On the role of intermolecular hydrogen bonding in miscible polymer blends. *Macromolecules* **1984,** *17* (9), 1671-1678.
68. Büttner, H.; Longwitz, L.; Steinbauer, J.; Wulf, C.; Werner, T., Recent Developments in the Synthesis of Cyclic Carbonates from Epoxides and CO2. *Top. Curr. Chem.* **2017,** *375* (3), 50.
69. Pinto da Silva, L., Mechanistic study of the role of hydrogen bond donors in the two-component organocatalysis of the ring-opening reaction of epoxides. *Mol. Catal.* **2019,** *474*, 110425.
70. Wurst, J. M.; Liu, G.; Tan, D. S., Hydrogen-Bonding Catalysis and Inhibition by Simple Solvents in the Stereoselective Kinetic Epoxide-Opening Spirocyclization of Glycal Epoxides to Form Spiroketals. *J. Am. Chem. Soc.* **2011,** *133* (20), 7916-7925.

## TOC image

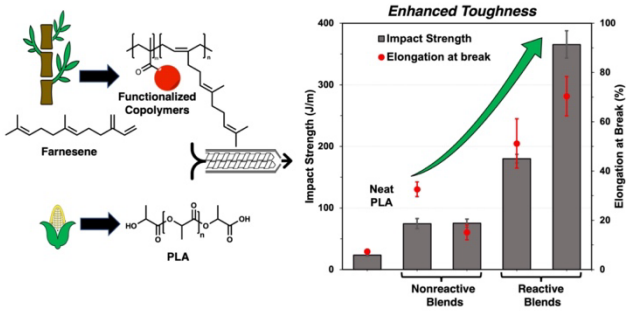
Functionalized
Copolymers
Farnesene
PLA
Enhanced Toughness
Impact Strength
Elongation at break
Neat
PLA
Impact Strength (J/m)
Elongation at Break (%)
Nonreactive
Blends
Reactive
Blends